Electronic Supplementary Material (ESI) for Nanoscale.

– Supplementary Information –

Thermal Hysteresis Controlled Reconfigurable MoS_2 Nanomechanical Resonators

Zenghui Wang[1,2†*], Rui Yang[1,3†*], Philip X.-L. Feng[1,4*]

[1]*Electrical Engineering, Case School of Engineering, Case Western Reserve University, Cleveland, Ohio 44106, USA*

[2]*Institute of Fundamental and Frontier Sciences, University of Electronic Science and Technology, Chengdu, China*

[3]*University of Michigan – Shanghai Jiao Tong University Joint Institute, Shanghai Jiao Tong University, Shanghai, China*

[4]*Department of Electrical & Computer Engineering, Herbert Wertheim College of Engineering, University of Florida, Gainesville, Florida 32611, USA*

[†]Equally Contributing Authors.

[*]Corresponding Authors. Emails: zenghui.wang@uestc.edu.cn, rui.yang@sjtu.edu.cn, philip.feng@ufl.edu

S1. Device Fabrication

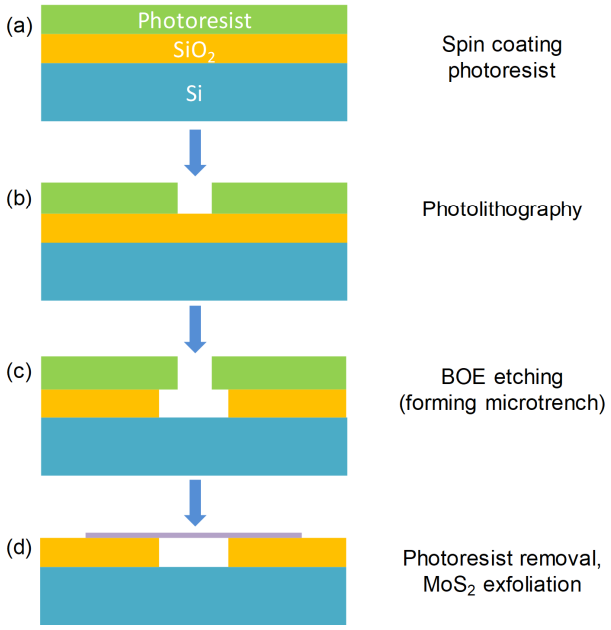

Figure S1. Device fabrication process for making the MoS_2 nanomechanical resonators.

Fabrication of the suspended MoS_2 nanomechanical resonators is performed by directly exfoliating MoS_2 crystal onto pre-patterned microtrenches[1] (Figure S1). Starting from the substrate of 290nm-thick thermal oxide (SiO_2) on Si, we pattern the wafer with standard photolithography, and define circular patterns with diameters of 0.8 μm to 5 μm (Figure S1b). Then we use buffered oxide etch (BOE) to remove the oxide, and control the etch time carefully (Figure S1c). After photoresist is removed, the substrate surface form arrays of microtrenches or cavities. We then perform mechanical exfoliation of MoS_2 onto the microtrenches, and then carefully search for the MoS_2 crystal that are freely suspended on the microtrenches under an optical microscope (Figure S1d).

S2. Resonance Measurement Techniques

We use a specially engineered laser interferometry system to detect the motion of the MoS_2 nanomechanical resonators with high sensitivity. We focus a 633 nm He-Ne laser with spot size of ~1 μm onto the surface of the MoS_2 resonator that is freely suspended onto the microtrench. The MoS_2 and the bottom surface of the microtrench form a microcavity, and when the MoS_2 vibrates out of plane, the vacuum gap between the MoS_2 and the substrate varies. The reflected light intensity is determined by the interferometry condition, and thus changes with the MoS_2

vibration. The signal is measured by a photodetector and then sent to a spectrum analyzer (for undriven motion detection) or a network analyzer (for driven resonance measurement). We can detect the undriven thermomechanical motion of the MoS_2 resonator using this laser interferometry system[1], as shown in Figure S2, using laser power of ~0.35 mW on device. To obtain the resonance frequency and Q, we fit the measured resonance data to the theoretical model,

$$S_v^{1/2}(\omega) = \left[\frac{a}{\left(\omega^2 - \omega_0^2\right)^2 + \omega^2\omega_0^2/Q^2} + (b\omega + c)^2 \right]^{1/2},$$

where $S_v^{1/2}(\omega)$ is the frequency-domain voltage spectral density measured by the spectrum analyzer, ω_0 is the angular resonance frequency of the MoS_2 resonator, Q is the quality factor of the resonator, ω is the sweeping frequency, a, b, and c are fitting parameters, and $(b\omega+c)^2$ is the frequency-dependent background response of the measurement system. The thermomechanical motion of a resonator in frequency domain is

$$S_{x,th}^{1/2}(\omega) = \left[\frac{4\omega_0 k_B T}{M_{eff} Q} \frac{1}{\left(\omega^2 - \omega_0^2\right)^2 + \omega^2\omega_0^2/Q^2} \right]^{1/2},$$

where T is temperature, k_B is Boltzmann's constant, M_{eff} is the effective mass of the nanomechanical resonator. The voltage domain signal due to thermomechanical motion is $S_{v,th}^{1/2} = \Re S_{x,th}^{1/2}$, where $\Re$ is the system responsivity of transducing displacement into voltage. The measured signal from the spectrum analyzer, or the total voltage-domain response is:

$$S_v^{1/2} = \left(S_{v,th} + S_{v,sys} \right)^{1/2},$$

where $S_{v,sys}$ is the noise power spectral density of the system background. Therefore,

$$S_v^{1/2}(\omega) = \left[\Re^2 \frac{4\omega_0 k_B T}{M_{eff} Q} \frac{1}{\left(\omega^2 - \omega_0^2\right)^2 + \omega^2\omega_0^2/Q^2} + S_{v,sys}(\omega) \right]^{1/2},$$

which can be simplified for fitting by using $a = \Re^2 \frac{4\omega_0 k_B T}{M_{eff} Q}$, and $S_{v,sys}^{1/2}(\omega) = b\omega + c$. For the thermomechanical resonance in Figure S2, from the fitting we obtain $\omega_0 = 2\pi f_0$, and f_0=21.8 MHz, Q=283. Then on resonance, $S_{x,th}^{1/2}(\omega_0) = \left(\frac{4k_B T Q}{\omega_0^3 M_{eff}} \right)^{1/2}$ =42.4 fm/Hz$^{1/2}$, assuming room temperature

T=300 K, and M_{eff}=0.1828M_0 for the fundamental flexural mode, where M_0 is the mass of the resonator in static state. From measured data in Figure S2, we know that on resonance, $S_{v,th}^{1/2} = \left(S_v - S_{v,sys}\right)^{1/2}$=0.056 μV/Hz$^{1/2}$, so $\Re$ =1.31 μV/pm.

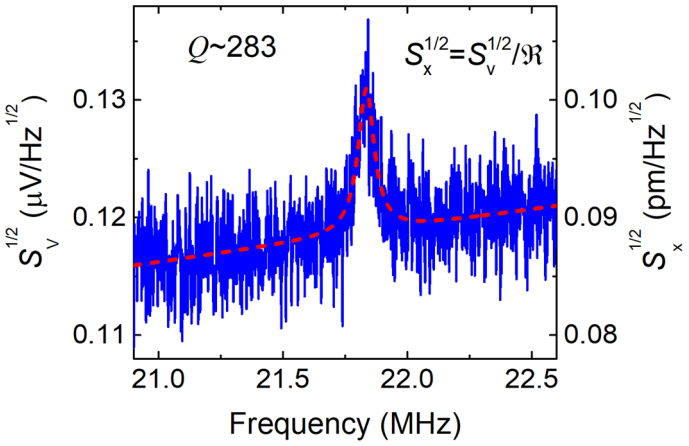

Figure S2. Measured undriven thermomechanical noise spectrum in voltage and displacement domain, for the MoS_2 device with a resonance at ~22MHz. The measured data (blue solid line) is the same as in Figure 2a in the Main Text, and the red dashed line shows the theoretical fitting as discussed above.

We also drive the device into large motion amplitude photothermally by using a 405 nm amplitude-modulated blue diode laser, with the radio-frequency (RF) modulation signal provided by a network analyzer[2]. The laser periodically heats up the MoS_2 crystal and the surrounding substrate to produce a thermal force for driving the resonator (*i.e.*, photothermal actuation). The driven resonances are typically easier to detect than the undriven thermomechanical resonances due to the larger vibration amplitudes, and we use driven resonances for our thermal pulse measurements. We use blue laser power of ~0.3 mW on device. The driven motion can also be measured interferometrically with the 633 nm laser, as shown in Figure 2b in the Main Text. We fit the driven resonance data to obtain the resonance frequency and Q, by using

$$A(\omega) = \left[\frac{a}{\left(\omega^2 - \omega_0^2\right)^2 + \omega^2\omega_0^2/Q^2}\right]^{1/2} + b\omega + c\,,$$

where $A(\omega)$ is the measured voltage from the network analyzer, a, b, and c are the fitting parameters, and the term $b\omega$+c accounts for the frequency-dependent system background.

S3. Resonances at Different Temperatures

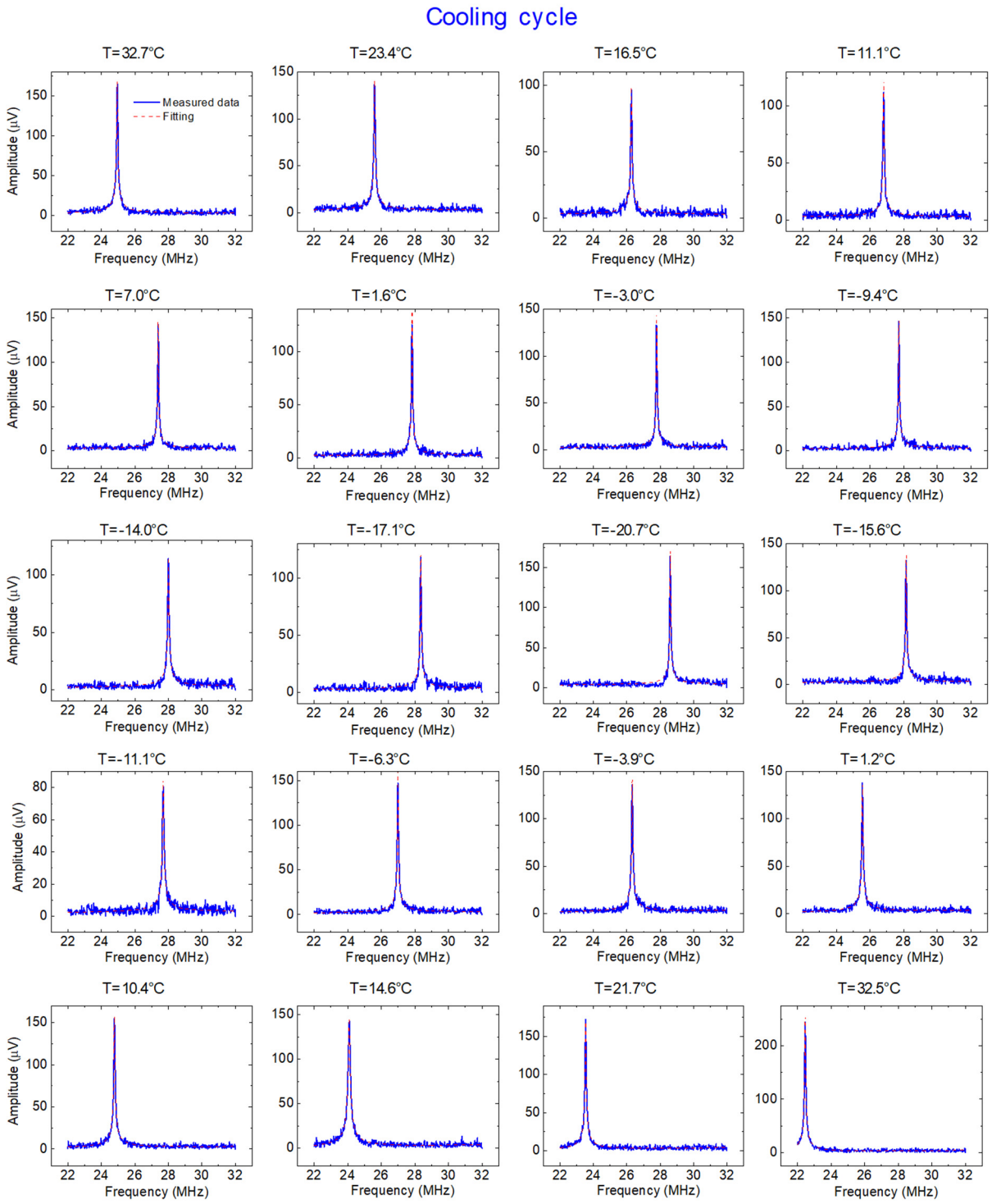

Figure S3. Resonances measured during the cooling cycle of the fully-sealed MoS_2 resonator.

We measure and record the resonances at different temperatures during the cooling cycle (Figure S3) and heating cycle (Figure S4), and perform theoretical fitting to each measured resonance curve and summarize the fitting-determined resonance frequency f_0 and Q at different temperatures in Table S1. When we change the substrate temperature, we wait for enough time until the temperature on the device stabilizes and the resonance frequency does not shift any more, and then record the resonance spectrum. Comparing the resonances before and after the cooling cycle in Figure S3, we observe clear differences in resonance frequency at ~32.5°C, due to the temperature hysteresis of the resonances[3]. We have also plotted the extracted Q versus varying temperature in Figure S5, and show the general trend of increasing Q with decreasing temperature, with fluctuations in Q.[4]

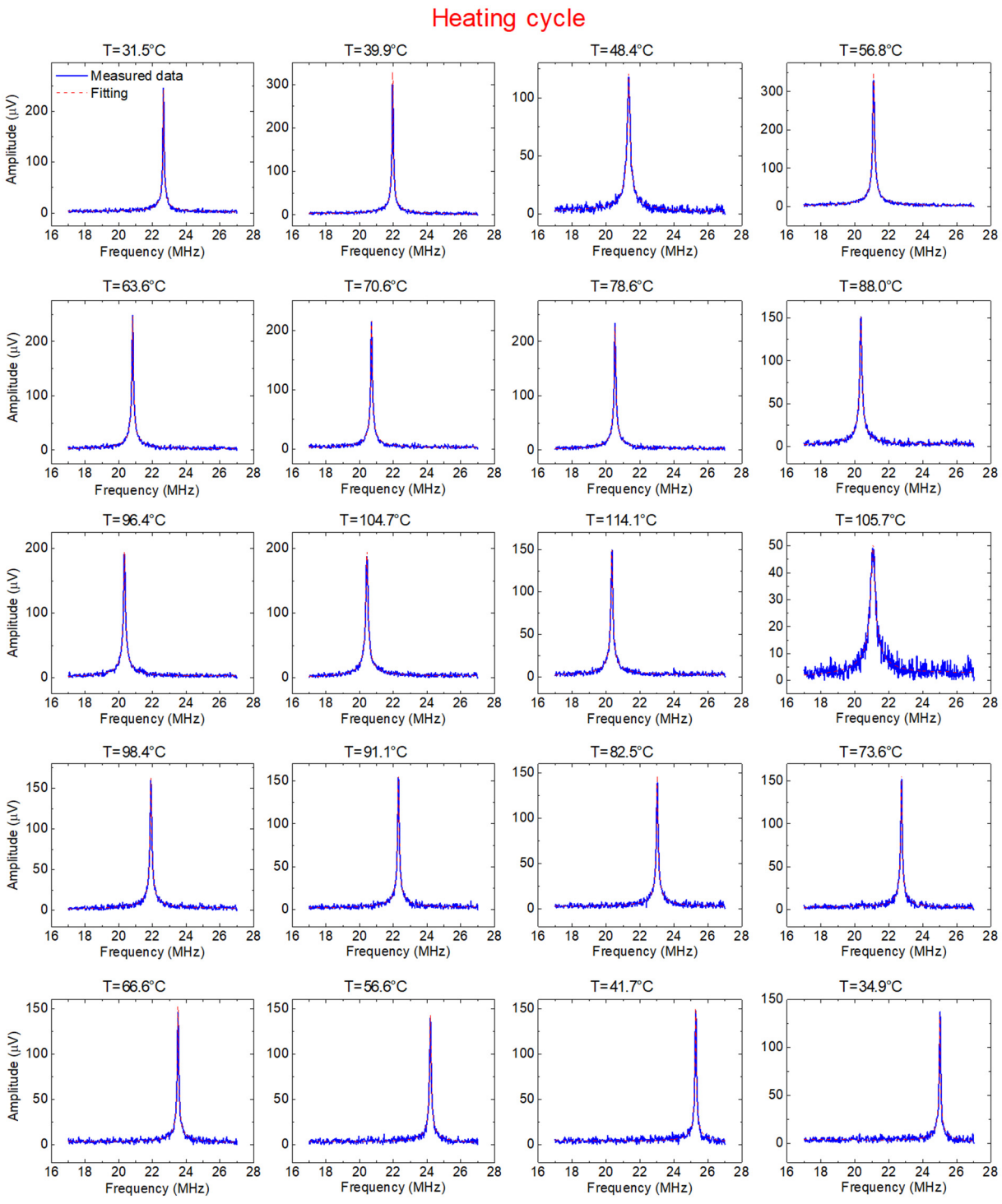

Figure S4. Resonances measured during the heating cycle of the fully-sealed MoS_2 resonator.

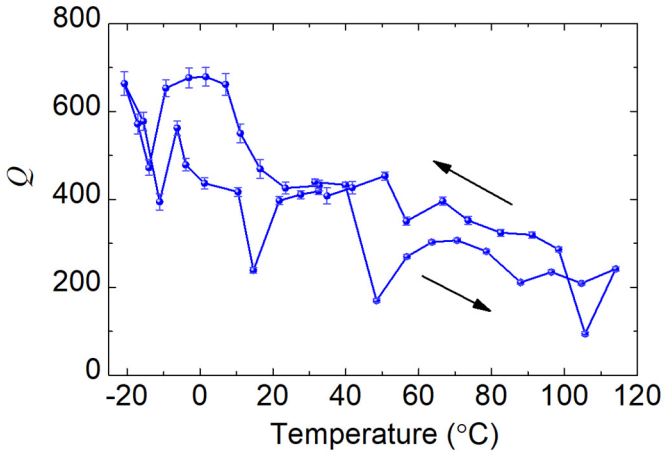

Figure S5. The extracted *Q* versus varying temperature with error bars in the resonance data fitting process, for the fully-sealed MoS_2 resonator measured in Figure S3 and Figure S4.

Table S1. Summary of measured f_0 and Q at different temperatures, for the MoS_2 resonator data shown in Figure S3 and Figure S4.

Cooling cycle			**Heating cycle**		
Temperature (°C)	f_0 (MHz)	Q	Temperature (°C)	f_0 (MHz)	Q
32.7	24.9	431	31.5	22.7	439
23.4	25.6	426	39.9	22.0	433
16.5	26.3	469	48.4	21.3	170
11.1	26.8	550	56.8	21.1	270
7.0	27.4	661	63.6	20.8	303
1.6	27.8	679	70.6	20.7	307
-3.0	27.8	676	78.6	20.5	282
-9.4	27.7	653	88.0	20.4	211
-14.0	28.0	472	96.4	20.3	235
-17.1	28.4	571	104.7	20.4	209
-20.7	28.6	663	114.1	20.3	242
-15.6	28.2	577	105.7	21.1	94
-11.1	27.7	394	98.4	21.9	286
-6.3	27.0	562	91.1	22.3	319
-3.9	26.3	478	82.5	23.0	324
1.2	25.6	436	73.6	22.7	352
10.4	24.8	417	66.6	23.5	396
14.6	24.1	238	56.6	24.2	350
21.7	23.5	397	50.8	24.7	453
27.6	22.9	411	41.7	25.3	426
32.5	22.5	418	34.9	25.0	408

S4. Power Estimation

We estimate the power consumption required to operate our switchable MoS_2 resonators, which consumes energy only for each switching operation (heating/cooling the device), while consuming zero power to maintain the resonance frequency once the switching is complete.

Toward future implementation, while peripheral circuit may be required to provide the current to heat up the device, with optimized design (such as using the device itself as the heater) the heater resistance is much larger than the components in series (so the heater takes most of the voltage drop) and much smaller than those connected in parallel (so most of the current flows through the heater). Therefore, most of the electrical power is dissipated by the heater (rather than other parts of the peripheral circuit) during heating. We also assume efficient local heating where approximately all the energy supplied contributes to the temperature increase of the device. The energy required to produce the heat pulse is calculated using $q=mc\Delta T$, where m is the mass of the MoS_2 resonator (which can be calculated using the device thickness, diameter, and MoS_2 mass density of 5060 kg/m^3), c is the heat capacity (395.3 J/(kg·K)[5]), and ΔT is the temperature difference (100 K for heating from 20°C to 120°C). For the device that is 56 nm thick, and 5 μm in diameter, we obtain $q=2.2\times10^{-10}$ J for each heating pulse.

For cooling pulse, we assume the cooling is provided by Carnot refrigerator, in which work needs to be done to the refrigerator in order to transport heat from the cold side to the hot side. The ratio between the heat removed from the cold end and the total work required, which is defined as the coefficient of performance (COP), is given by: $COP=T_L/(T_H-T_L)$, where T_H and T_L are the temperatures of the hot and cold sides of the refrigerator, measured in Kelvin. In our case, the cooling is from 20°C to -20°C, and we calculate COP≈6.3, suggesting that *in principle* cooling can be achieved rather efficiently in the temperature range. In our particular case, the energy required for a cooling pulse is on the same order as that for a heating pulse (or even less). Therefore, we use the energy required for a heating pulse calculated above for the subsequent comparison.

We now estimate the power consumption of voltage-tuned NEMS resonators (Figure S6). In this scheme, a voltage needs to be continuously applied to a bias electrode (such as the gate) of the resonator to sustain the resonance frequency. While the bias electrode can be assumed to have zero leakage to other electrodes, the peripheral circuit that supplies the voltage is composed of transistors, which has finite leakage current even in the off state. To date, some of the CMOS

design can achieve an infinitesimal off-state leak current on the order of 80 pA through the source/drain[6]. Assuming a 10 V voltage is applied to tune the resonance frequency, the power dissipated from leakage through a single transistor path is 8×10^{-10} W. Assuming during switching operation the bias voltage is applied half of time on average, then the averaged power consumption due to application of bias voltage is 4×10^{-10} W.

Below we compare the minimal required power for operating both types of switchable resonators by including energy consumption for both switching and maintaining the frequency. Since in the thermal-pulse tunable resonators, energy is consumed only when the resonator is switched each time but not during the maintaining part, the average power decreases as the switching period increases. In contrast, in conventional voltage-controlled tunable resonators, power is dissipated during both the switching and maintaining portions because there is always a voltage applied, thus the average power does not depend on the rate the resonator is switched, but only depends on the portion of total time when the voltage is applied.

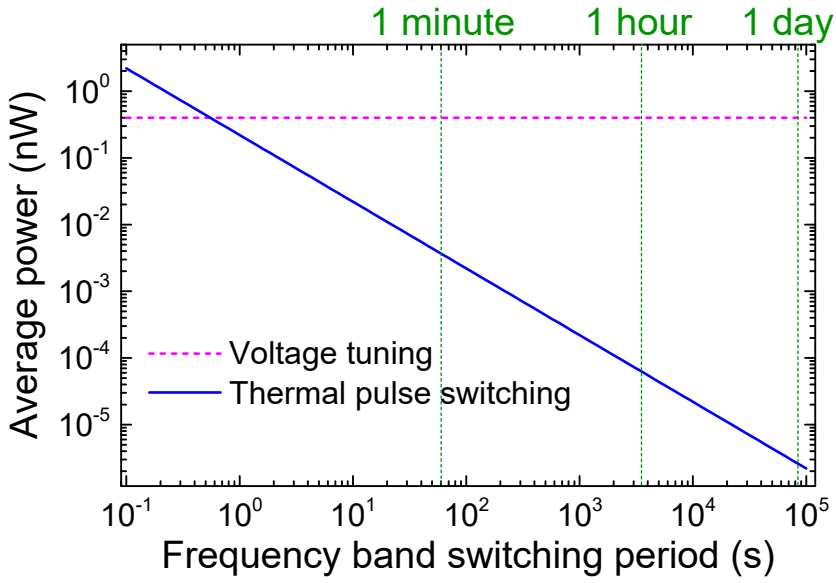

Figure S6. Comparison of average power consumption for thermal pulse switching and voltage tuning.

S5. Switching Time Simulation

The tuning time can be shortened by using local heaters, instead of heating the whole chip substrate. Currently, we use a global heater to heat up the chip substrate, and the heat needs to transfer through the chip substrate to reach the MoS_2 device, which results in a relatively long

thermal tuning time. Through finite element simulation, we show that, by using localized heaters close to the MoS_2 layer (Figure S7a), we expect to maintain the frequency tuning capability (Figure S7b), while having much shorter thermal tuning time. As shown in Figure S7c-d, by using local heaters, we just need 100 μW heating power to heat up the device to ~120 °C, and after 10 ms time the temperature on MoS_2 already stabilizes, showing that the heating speed can be improved by local on-chip heaters.

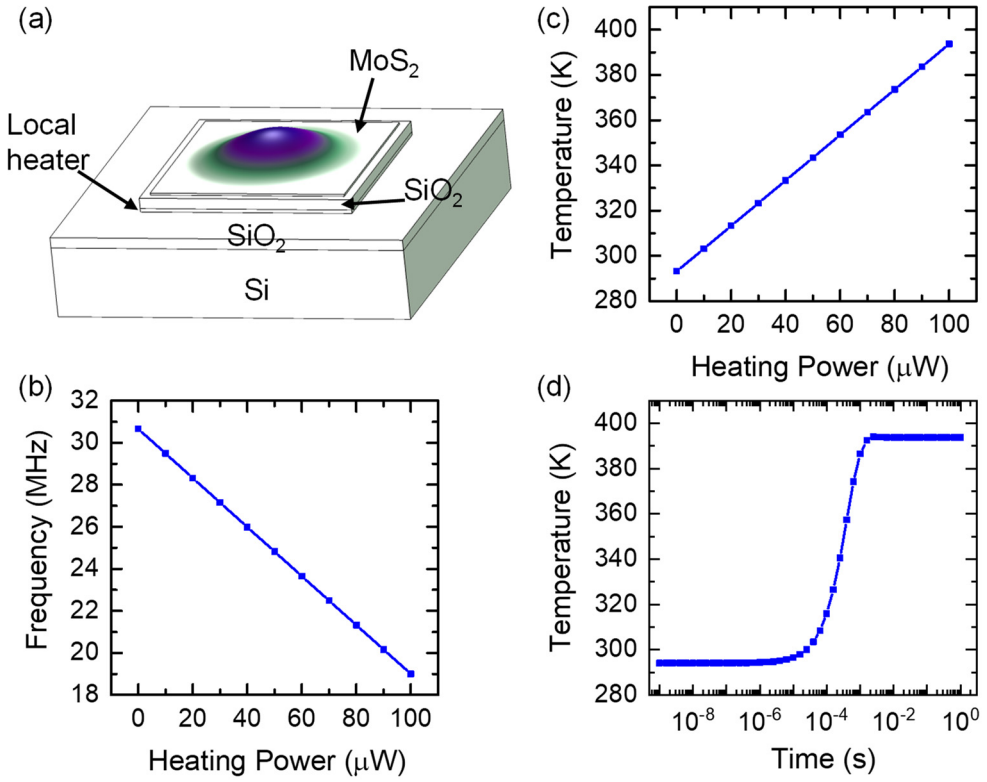

Figure S7. Finite element simulation of a MoS_2 resonator with a local heater. (a) Simulated fundamental resonance mode shape and the device structural layers. (b) Frequency shift with increasing heating power. (c) Average temperature of MoS_2 at different heating power. (d) Transient response of average temperature on MoS_2 with heating power of 100 μW, showing that the temperature already stabilizes after 10 ms.

S6. Other MoS_2 Resonators with Thermal Hysteresis

We have also measured other MoS_2 resonators that clearly show thermal hysteresis. Using the partially-sealed device as in Figure 2e-g in the Main Text which does not show thermal hysteresis, we measure it at higher pressure of 90 Torr. It is interesting to find that the device exhibits thermal

hysteresis (Figure S8a) at this higher pressure; and the room-temperature (25°C) resonance frequencies are different during cooling (Figure S8b) and heating cycles (Figure S8c), at this higher pressure of 90 Torr. As the higher pressure (lower vacuum) offers more available adsorbates that can interact with the device surface, this (and its contrast to data from lower pressure) further indicates that the suggested temperature-programmed adsorption–desorption process is likely responsible for the observed thermal hysteresis.

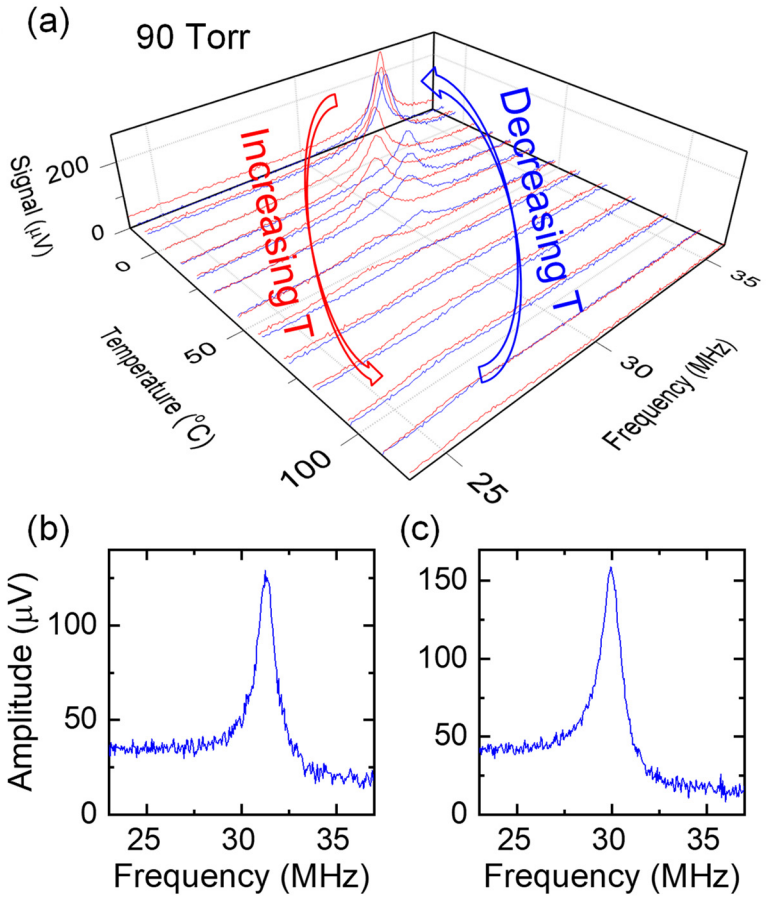

Figure S8. Frequency response and thermal hysteresis measured from the partially-sealed MoS_2 resonator described in Figure 2e-g in the Main Text, measured at 90 Torr, clearly demonstrating (a) temperature hysteresis of the MoS_2 resonator, (b)-(c) driven resonances at 25°C when temperature (b) sweeps down, and (c) sweeps up, exhibiting different resonance frequencies.

References

1. J. Lee, Z. Wang, K. He, J. Shan, and P. X.-L. Feng, High frequency MoS_2 nanomechanical resonators. *ACS Nano*, 2013, **7**, 6086-6091.

2. J. Lee, Z. Wang, K. He, R. Yang, J. Shan, and P. X.-L. Feng, Electrically tunable single- and few-layer MoS_2 nanoelectromechanical systems with broad dynamic range. *Science Advances*, 2018, **4**, eaao6653.

3. Z. Wang, R. Yang, A. Islam, and P. X.-L. Feng, Observation of strong temperature hysteresis in molybdenum disulfide (MoS_2) vibrating nanomechanical resonators. In *Proc. IEEE Int. Frequency Control Symposium & European Frequency and Time Forum (IFCS-EFTF 2015)*, 2015, pp. 783-786.

4. Y. T. Yang, C. Callegari, X. L. Feng, and M. L. Roukes, Surface adsorbate fluctuations and noise in nanoelectromechanical systems. *Nano Letters*, 2011, **11**, 1753-1759.

5. A. Sood, *et al.*, Quasi-ballistic thermal transport across MoS_2 thin films. *Nano Letters*, 2019, **19**, 2434-2442.

6. E. Sicard, Introducing 14-nm FinFET technology in Microwind. *Microwind Application Note* 2017, hal-01541171.